
GOLDENE MONOLAYER AS A HIGHLY EFFECTIVE CATALYST FOR POLYSULFIDE ANCHORING AND CONVERSION: A THEORETICAL STUDY

AN ARXIV PREPRINT

 **Nicolas F. Martins**¹,  **José A. dos S. Laranjeira**¹,  **Bill D. A. Huacarpuma**²  **Kleuton A. L. Lima**³,
 **Luiz A. Ribeiro Jr**^{3,†}, and  **Julio R. Sambrano**¹,

¹Modeling and Molecular Simulation Group, São Paulo State University (UNESP), School of Sciences, Bauru 17033-360, SP, Brazil

²Computational Materials Laboratory, LCCMat, Institute of Physics, University of Brasília, 70910-900, Brasília, Federal District, Brazil

³Department of Applied Physics and Center for Computational Engineering and Sciences, State University of Campinas, Campinas, 13083-859, SP, Brazil

  *nicolas.ferreira@unesp.br

  [†]jr.sambrano@unesp.br

January 9, 2026

ABSTRACT

We use first-principles density functional theory to investigate how lithium sulfide and polysulfide clusters (Li_2S , Li_2S_2 , Li_2S_4 , Li_2S_6 , Li_2S_8 , and S_8) bind to Goldene, a new two-dimensional gold allotrope. All $\text{Li}-\text{S}$ species exhibit robust binding to Goldene. The adsorption energies range from -4.29 to -1.90 eV. S_8 that is alone interacts much less strongly. Charge density difference and Bader analyses indicate that substantial charge is transferred to the substrate, with a maximum 0.92 e for Li -rich clusters. This transfer induces polarization at the interface and shifts the work function to 5.30 - 5.52 eV. Projected density-of-states calculations indicate that $\text{Au-}d$ and $\text{S-}p$ states strongly mix near the Fermi level. This hybridization indicates that the electronic coupling is strong. Based on these results, the reaction free-energy profile for the stepwise conversion of S_8 to Li_2S on Goldene is thermodynamically favorable. The overall stabilization is -3.64 eV, and the rate-determining barrier for the $\text{Li}_2\text{S}_2 \rightarrow \text{Li}_2\text{S}$ step is 0.47 eV. This shows that Goldene is an effective surface for anchoring and mediating lithium polysulfide reactions.

Keywords borospherene · borophene · DFT · gas sensing · 2D materials.

1 Introduction

Because of their low environmental impact, high theoretical energy density, and the natural abundance of sulfur, lithium-sulfur (Li-S) electrochemical systems have attracted significant interest [1, 2]. The dissolution and migration of lithium polysulfides (Li_2S_x , $2 \leq x \leq 8$) and interfacial instability during cycling are two intrinsic challenges that limit practical implementation despite these benefits [3]. Low Coulombic efficiency and rapid capacity fading are caused by these issues, especially the uncontrolled movement of soluble polysulfides between electrodes [4, 5]. As a result, interfacial engineering becomes an essential tactic for improving performance.

Two-dimensional (2D) materials are increasingly used as platforms for anchoring polysulfide and mediating reactions because they offer large surface areas, can be tuned to alter their electronic structure, and can react with a wide range of chemicals [6–9]. Graphene-based materials were among the first studied in this context because they exhibit high electrical conductivity and mechanical stability [10–12]. However, because pristine graphene is nonpolar, lithium polysulfides do not adhere well to it [13]. To address this limitation, several functionalization strategies have been proposed to enhance chemical affinity, but they often come at the cost of increased structural complexity or reduced conductivity [14, 15].

On the other hand, transition-metal dichalcogenides such as MoS_2 have polar surfaces that can form stronger chemical bonds with lithium polysulfides [16, 17], since exposed metal sites increase the adsorption energies and catalytic activity in polysulfide conversion reactions. The MXenes family is another class of nanomaterials explored as potential anchoring surfaces because they are good electrical conductors, have hydrophilic surfaces, and exhibit a strong affinity for sulfur species [18, 19]. Liang and coworkers [20] found that applying a fluorine-free fabrication of Ti_3C_2 MXenes reduces the environmental impact of MXene synthesis and also promotes electron reservoirs due to the reactive oxygen species on the terminated surface. From a catalytic perspective, Fang and colleagues [21] executed a screening of 27 potential MXene cathodes for Li–S batteries based on density functional theory (DFT). They obtained Ti_2CS_2 , Mo_2CS_2 , and W_2CS_2 as promising catalysts due to the less endothermic Gibbs free energies during the rate-determining step from Li_2S_2 to Li_2S . Other studies have also examined the effect of S- or Se-terminated MXenes on polysulfide conversion [22, 23].

The recent synthesis of Goldene, a 2D monolayer allotrope of gold, has created new possibilities for designing interfacial materials [24]. As a metallic 2D material with high electrical conductivity, structural robustness, and exposed Au atoms, Goldene offers new possibilities for a myriad of applications. Specifically, Kumar and coworkers [25] proposed the functionalization of the Goldene monolayer with different metal adatoms to enhance the Co_2 activation. Sheremeteva and Meunier, for example, found that Goldene supports a high coverage ratio of adsorbed hydrogen atoms, which could amplify research in the field of catalysis and hydrogen storage with Au-based surfaces. Different theoretical efforts have also been executed to investigate an overview of the main structural and electronic properties of Goldene [26–28]. However, there are no reports on the potential use of the Goldene monolayer as an anchoring material to enhance polysulfide conversion. Additionally, it is well documented that Au-based nanomaterials strongly interact with sulfur-containing species [29–31]. This indicates that Goldene can enhance the charge–discharge mechanism of Li–S batteries by combining the promising properties of the noble metal Au with the unique attributes of 2D materials.

In this work, we present a systematic first-principles investigation of the adsorption, electronic structure, and reaction energetics of lithium sulfide and polysulfide clusters (Li_2S_n , where $n = 1, 2, 4, 6$, and 8) on Goldene. By combining adsorption energy analysis, charge density difference (CDD), work-function modulation, projected density of states, and reaction free-energy profiling, we elucidate the fundamental mechanisms governing Li–S interactions at the Goldene interface. Our results position Goldene as a promising metallic 2D platform for controlling polysulfide chemistry and reaction pathways at the nanoscale.

2 Computational Methods

All calculations were conducted using density functional theory (DFT) as executed in the Vienna ab initio Simulation Package (VASP) [32]. The projector-augmented-wave (PAW) method [33] was used to describe the interactions between valence electrons and ionic cores. Simultaneously, exchange-correlation effects were accounted for using the generalized gradient approximation within the Perdew–Burke–Ernzerhof (PBE) framework [34, 35]. To ensure that the total energies and electronic properties were correct, a plane-wave kinetic energy cutoff of 520 eV was used.

Goldene was modeled as a 2D slab with periodic boundary conditions applied in the in-plane directions. A vacuum spacing of 20 Å was introduced along the out-of-plane direction to avoid spurious interactions between periodic images. Structural optimizations were carried out using a Γ -centered $6 \times 6 \times 1$ Monkhorst–Pack k -point mesh, while a denser

$10 \times 10 \times 1$ grid was adopted for electronic structure and projected density of states (PDOS) calculations. Long-range dispersion interactions were accounted for using the DFT-D3 method [36].

All atomic positions were fully relaxed until the total energy variation between ionic steps was below 10^{-5} eV and the residual Hellmann–Feynman forces on each atom were smaller than 0.01 eV/Å. S_8 and Li_2S_n ($n = 1, 2, 4, 6$, and 8) clusters were initially placed above the Goldene surface in multiple orientations, and the most stable adsorption geometries were identified through total energy minimization.

The adsorption energy (E_{ads}) of each cluster on Goldene was calculated using the following equation:

$$E_{ads} = E_{Goldene+cluster} - E_{Goldene} - E_{cluster}. \quad (1)$$

where $E_{Goldene+cluster}$, $E_{Goldene}$, and $E_{cluster}$ represent the total energies of the combined system, the pristine Goldene monolayer, and the isolated Li–S cluster, respectively. Negative values of E_{ads} indicate energetically favorable adsorption.

The elementary reaction steps involved in the formation of a single Li_2S molecule are described as follows:



Here, the superscript * denotes adsorption at an active site on the substrate. The Gibbs free energy change ΔG associated with each elementary step is calculated using the following expression:

$$\Delta G = \Delta E + \Delta E_{ZPE} - T\Delta S, \quad (7)$$

where ΔE represents the adsorption energy, while ΔE_{ZPE} and $T\Delta S$ correspond to the zero-point energy and entropy differences between products and reactants, respectively. These quantities were obtained from vibrational frequency calculations performed at 298 K. In this work, ΔE_{DFT} was determined from the difference in total energies of the adsorbed intermediate states before and after each elementary reaction step. The terms ΔE_{ZPE} and ΔS correspond to the variations in zero-point vibrational energy and entropy, respectively, evaluated at 298.15 K. Previous theoretical investigations on Li–S battery systems have shown that the contributions of ΔE_{ZPE} and $T\Delta S$ are relatively small and can be safely neglected [37, 38]. Consequently, the Gibbs free energy change can be reasonably approximated as $\Delta G \approx \Delta E_{DFT}$.

3 Results and Discussion

3.1 Structural description

Figure 1 illustrates the structural models employed in this work. Panel (a) displays the optimized Goldene monolayer used as the two-dimensional substrate, with the in-plane lattice parameters highlighted as 2.76 Å and 4.70 Å along the indicated crystallographic directions. The dashed outline denotes the simulation cell adopted for the periodic calculations. Panel (b) presents the electronic band structure of the Goldene monolayer, confirming its intrinsic metallic character, as evidenced by multiple bands crossing the Fermi level (set to 0 eV). This metallicity is a key attribute for its investigation as a promising platform for Li–S batteries, since high electrical conductivity is essential to enhance charge–discharge kinetics and suppress the shuttle effect. Finally, panel (c) shows the isolated and fully optimized

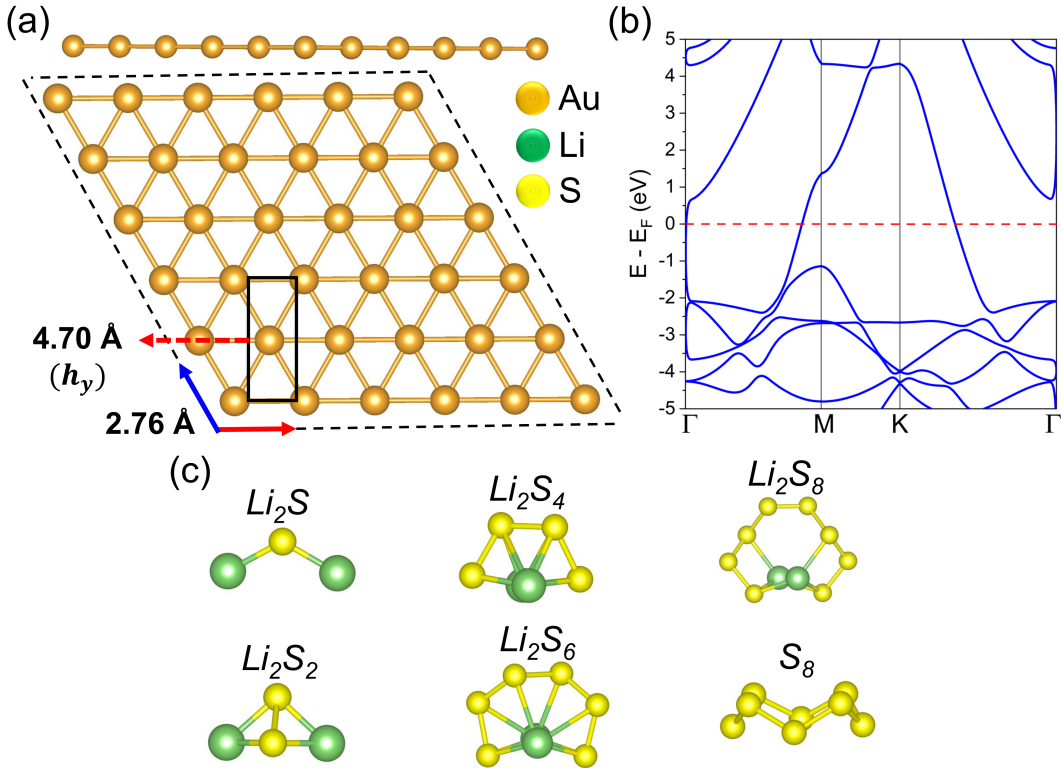


Figure 1: (a) Top and side views of the optimized Goldene monolayer and (b) its electronic band structure, with the Fermi level set to 0 eV. (c) Fully optimized isolated sulfur-containing species considered in this study, including Li_2S , Li_2S_2 , Li_2S_4 , Li_2S_6 , Li_2S_8 , and S_8 .

sulfur-containing species considered in this study— Li_2S , Li_2S_2 , Li_2S_4 , Li_2S_6 , Li_2S_8 , and S_8 —which serve as molecular and cluster building blocks for the subsequent interfacial calculations.

We further evaluated the mechanical properties of the Goldene monolayer by calculating its elastic constants (C_{11} , C_{12} , C_{22} , and C_{66}), as well as the polar representations of Young's modulus (Y) and Poisson's ratio (ν), as shown in Figure 2. The calculated stiffness constants are 103.56 N/m (C_{11}), 34.71 N/m (C_{12}), 95.22 N/m (C_{22}), and 28.11 N/m (C_{66}), indicating a higher mechanical rigidity compared to Goldene analogs such as copperene and silverene [27]. The polar plots in Figure 2 reveal a pronounced anisotropic mechanical behavior, with a maximum Young's modulus of 90.90 N/m and a maximum Poisson's ratio of 0.41. These results demonstrate that Goldene exhibits a robust mechanical response, highlighting its suitability for applications in energy storage systems.

3.2 Interaction of S_8 and Li_2S_n ($n = 1, 2, 4, 6$, and 8) clusters

To see if Goldene can work as a cathode material, we first look at how it interacts with sulfur-containing compounds. Figure 3 shows the most stable ways in which lithium sulfide and lithium polysulfide clusters can adhere to the Goldene surface. All Li–S species create stable energy configurations, which means that Goldene can hold polysulfides in place over a wide range of chain lengths. It is possible to identify that all Li_2S_n clusters, including the S_8 molecule, maintain the molecular shape visualized in Figure 1b. This finding is important since the cathode materials should capture the LiPS without dissociating or degrading the polysulfide species.

Our results indicate that all LiPS are strongly adsorbed on the Goldene surface, suggesting the remarkable effect of the Au atom in interacting with the polysulfides to enhance the binding affinity. The adsorption energy results, also included in Figure 3, corroborate the previous observation. The energy ranges from -1.90 to -4.29 eV, with the largest

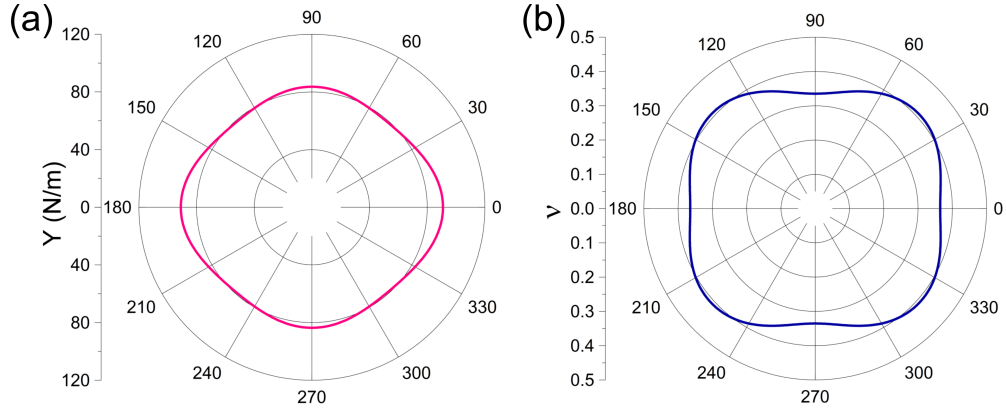


Figure 2: (a) Young's moduli and (b) Poisson's ratio for Goldene monolayer.

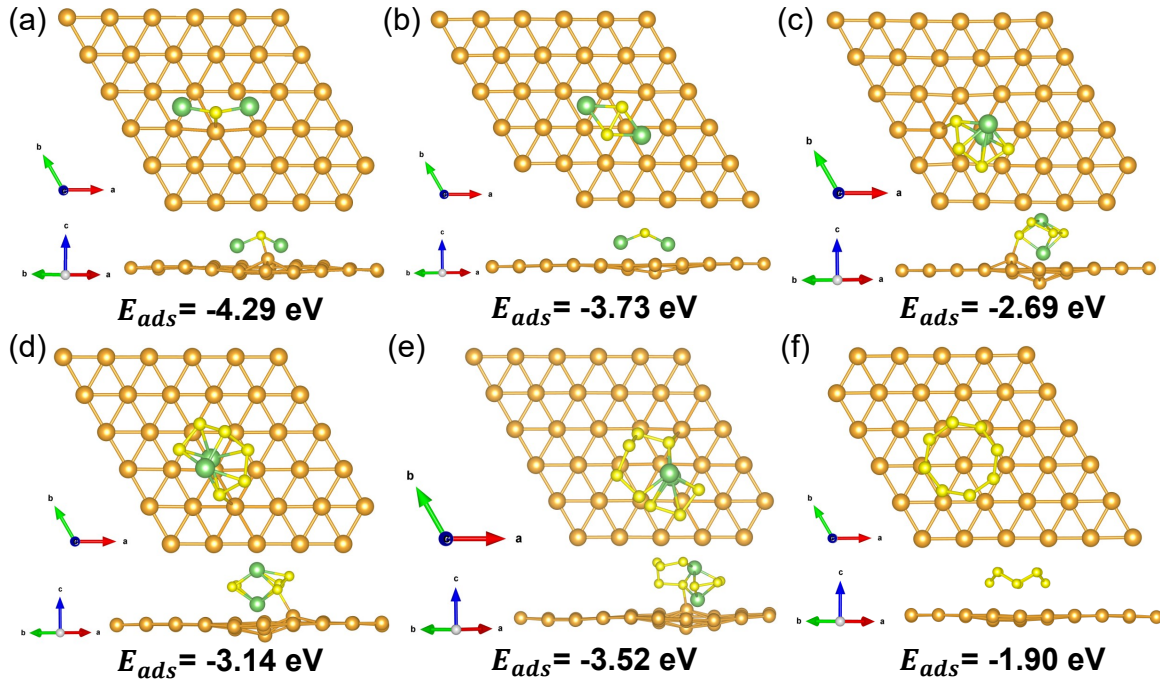


Figure 3: Optimized adsorption configurations of Li_2S_n and S_8 clusters on Goldene, together with their corresponding adsorption energies (E_{ads}). Panels (a)–(f) show the most stable geometries for Li_2S , Li_2S_2 , Li_2S_4 , Li_2S_6 , Li_2S_8 , and S_8 , respectively, viewed from the top and side.

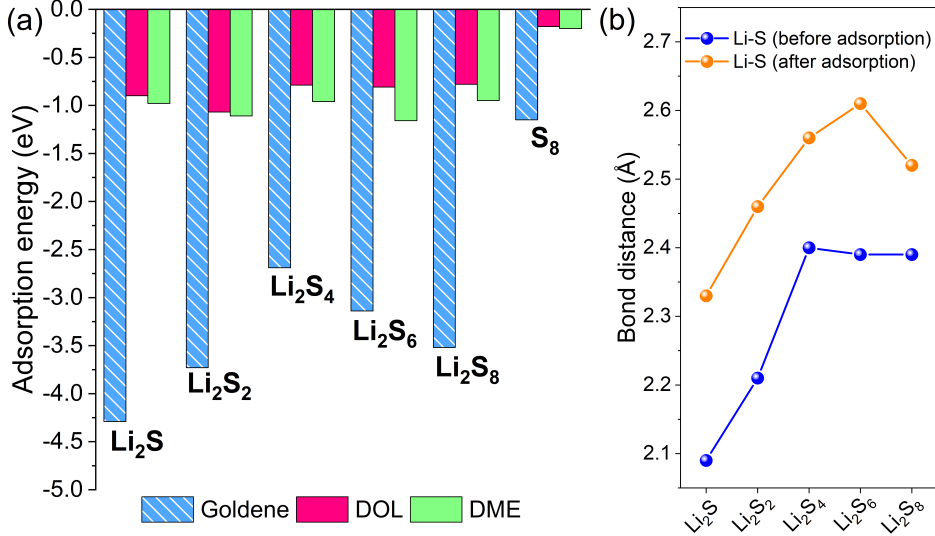


Figure 4: (a) Comparison of adsorption energies (E_{ads}) of Li_2S_n and S_8 cluster species on Goldene and in common organic electrolyte solvents (DOL and DME), and the (b) Li-S bond distances before and after each lithium polysulfide adsorption on Goldene.

negative energy values being computed for Li_2S ($E_{ads} = -4.29$ eV) and Li_2S_2 ($E_{ads} = -3.73$ eV). Low-sulfur chains like Li_2S and Li_2S_2 are expected to present higher interaction energies due to the contribution of both Li atoms in the final anchoring (see Figures 3a and b). On the other hand, the computed adsorption energies slightly decrease as the sulfur concentration increases. In general, the Goldene monolayer presents substantial binding strength for polysulfides compared to graphene and other graphene-based materials, which usually show adsorption energies lower than 2 eV (in absolute values) [39–41].

From a practical point of view, it is important that lithium polysulfide binds strongly to the cathode surface so that it does not dissolve into the electrolyte. The adsorption energies of lithium polysulfides in common organic solvents such as 1,3-dioxolane (DOL) and 1,2-dimethoxyethane (DME) are typically between -0.18 and -1.16 eV [42], which are much weaker than the values we found for Goldene (see Figure 4). This comparison indicates that, upon lithiation, sulfur-containing species preferentially remain adsorbed on the Goldene surface rather than dissolve into the electrolyte, which is essential for reducing the shuttle effect and improving cycling stability in Li–S systems.

This comparison indicates that, upon lithiation, sulfur-containing species preferentially remain adsorbed on the Goldene surface rather than dissolve into the electrolyte, which is essential for reducing the shuttle effect and improving cycling stability in Li–S systems. For rapid kinetics during polysulfide conversion, particularly in the formation of the final product (Li_2S^*), cleavage of the Li–S bond is required [43, 44]. As shown in Fig. 4b, a clear stretching of the Li–S bond is observed for all Li_2S_n clusters. This effect is more pronounced for low-sulfur species (Li_2S and Li_2S_2), where Li atoms migrate across the Goldene surface to delocalize electrons owing to their strong donor character. This behavior leads to elongation of the Li–S bond length and consequently promotes faster lithium kinetics.

To complement the structural results, Bader charge analysis and charge density difference (CDD) maps were computed for S_8 and all Li_2S_n clusters. The CDD was obtained using the following expression:

$$\Delta\rho(\mathbf{r}) = \rho_{\text{Goldene}+\text{cluster}}(\mathbf{r}) - \rho_{\text{Goldene}}(\mathbf{r}) - \rho_{\text{cluster}}(\mathbf{r}). \quad (8)$$

Figure 5 shows the obtained CDD maps for each configuration along with the amount of charge transferred. This figure provides a direct view of how interfacial interactions alter the electronic structure. In all cases, there is a clear buildup of electron density at the interface between sulfur atoms and the Goldene surface. There are also clear charge depletion

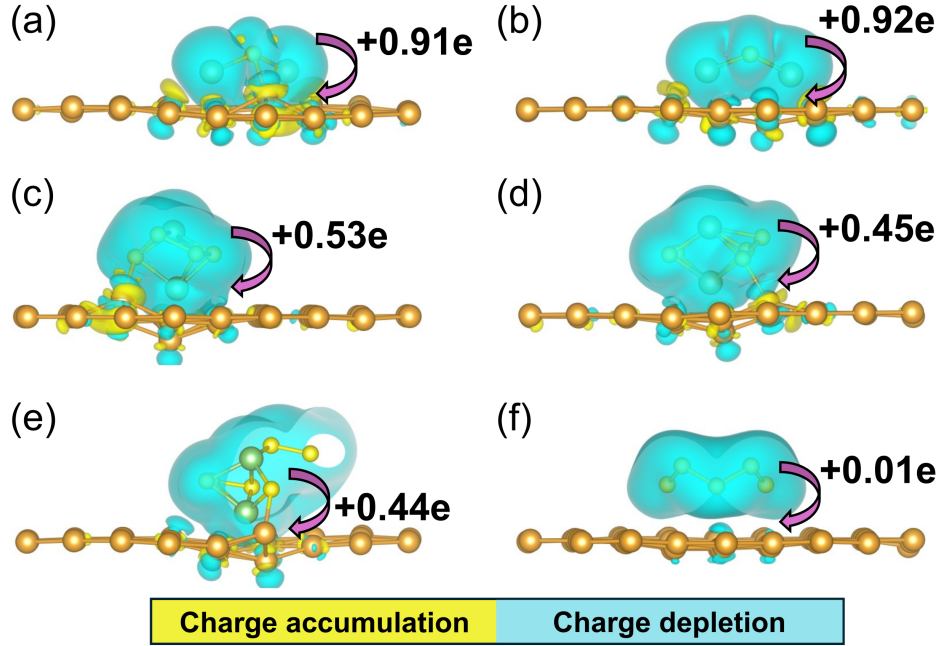


Figure 5: Charge density difference (CDD) plots for Li_2S_n and S_8 clusters adsorbed on Goldene. Panels (a)–(f) correspond to Li_2S , Li_2S_2 , Li_2S_4 , Li_2S_6 , Li_2S_8 , and S_8 , respectively. Yellow and cyan isosurfaces represent charge accumulation and depletion, respectively, induced by adsorption.

regions around lithium atoms in the clusters. This pattern shows that charge is moving from the Li–S species to the Goldene substrate. Bader charge analysis shows that the amount of charge transferred depends on the number of lithium atoms in the cluster and how they connect to the rest of the cluster. As expected, Li_2S and Li_2S_2 exhibit the greatest charge transfer, reaching about 0.91 e and 0.92 e , respectively, indicating that these species are highly ionic and have strong electronic interactions with the Goldene surface. The transferred charge decreases as the sulfur chain lengthens: it ranges from 0.53 e for Li_2S_4 to 0.45 e for Li_2S_6 and 0.44 e for Li_2S_8 . This means that the charge is spreading out more within the polysulfide structure and that each lithium atom contributes less charge to the interface. On the other hand, the significant contribution of vdW forces on the S_8 adsorption induces an almost negligible charge transfer from this cluster to the Goldene monolayer. Finally, we can attest that our charge-transfer analysis is closely linked to the previous results concerning the binding strength of polysulfides on Goldene.

To clarify the electronic interactions between sulfur-containing species and the Goldene substrate, projected density-of-states calculations were conducted, as illustrated in Figure 6. The PDOS profiles show that Goldene maintains its metallic character in all cases, even though lithium sulfide and polysulfide clusters adhere to it well. There are still many Au d states at the Fermi level, indicating that the adsorption process does not compromise the substrate’s excellent electronic conductivity. This is an important requirement for cathode materials in Li–S systems. In Li-containing species, significant hybridization between Au d and S p states occurs near the Fermi level, especially in Li_2S and Li_2S_2 . This overlap indicates that chemical Au–S bonds are forming, consistent with the short interfacial distances and high adsorption energies. As the length of the polysulfide chain increases, the contribution of S p states near the Fermi level becomes more spread out. This is because sulfur orbitals in longer chains are less localized; yet, they still interact with the Goldene surface.

Another important descriptor for evaluating the modulation of a surface’s reactivity is the work function (Φ) of the substrate, which quantifies the minimum energy required to extract an electron from the Fermi level to the vacuum level

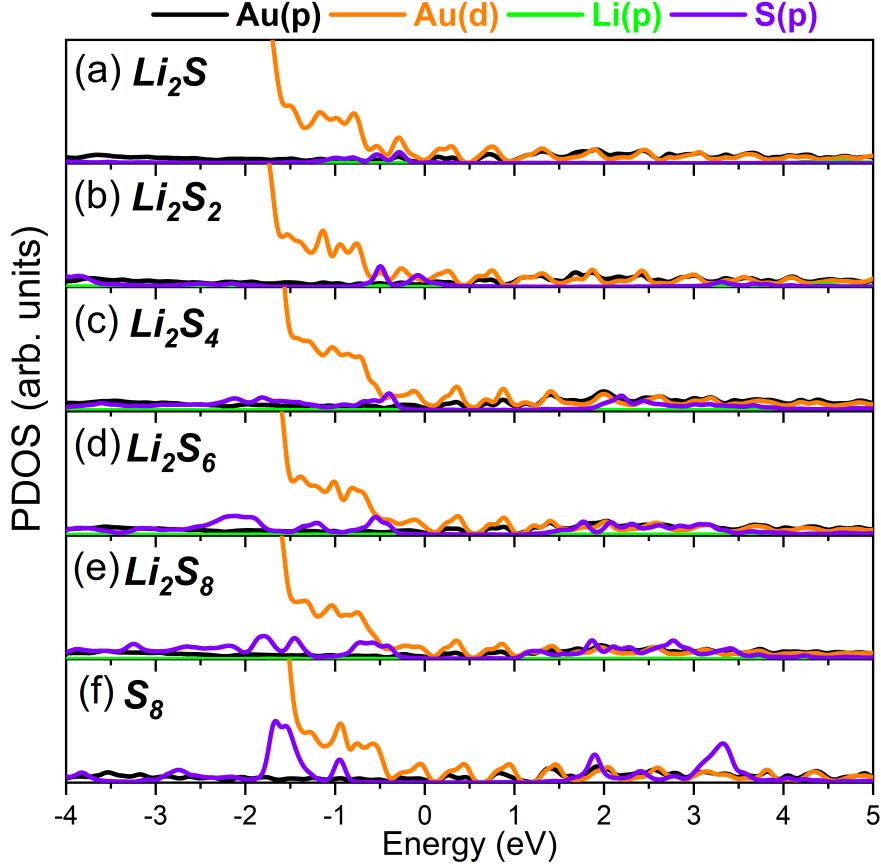


Figure 6: Projected density of states (PDOS) for Goldene with adsorbed lithium sulfide and polysulfide species. Panels (a)–(f) correspond to Li_2S , Li_2S_2 , Li_2S_4 , Li_2S_6 , Li_2S_8 , and S_8 , respectively. Contributions from Au p and d , Li p , and S p orbitals are shown. The Fermi level is set to zero energy.

[45, 46]. From a theoretical perspective, the work function is calculated according to

$$\Phi = V_\infty - E_F, \quad (9)$$

where V_∞ represents the vacuum-level electrostatic potential and E_F corresponds to the system's Fermi energy. Here, we assessed (Φ) by computing the planar-averaged electrostatic potentials, where the distances were considered along the vertical z -direction with $V(z) = \pm\infty$, as visualized in Figure 7. Pristine Goldene exhibits a work function of 5.50 eV, reflecting its intrinsic metallic character. Upon introducing lithium polysulfides at the Goldene interface, pronounced asymmetric peaks emerge along the positive z -axis, indicating that the interaction with Li_2S_n clusters perturbs the Goldene surface. Consequently, Φ decreases for all lithium polysulfide species, with reductions of 0.10, 0.13, 0.20, 0.15, and 0.14 eV for Li_2S , Li_2S_2 , Li_2S_4 , Li_2S_6 , and Li_2S_8 , respectively. This behavior illustrates the charge redistribution mechanisms discussed above. Lithium-based clusters donate electrons to the gold surface, thereby creating an interfacial layer that alters the electrostatic potential and reduces the work function. In contrast, due to the weak adsorption of S_8 on the Goldene monolayer, its work function is only slightly shifted to 5.52 eV.

3.3 Catalytic potential of Goldene during charge-discharge reaction

In this work, the sulfur reduction reaction (SRR) is examined by calculating the Gibbs free energy changes (ΔG) along the charge–discharge pathway, which comprises a sequence of reactions from S_8 to the formation of Li_2S . This

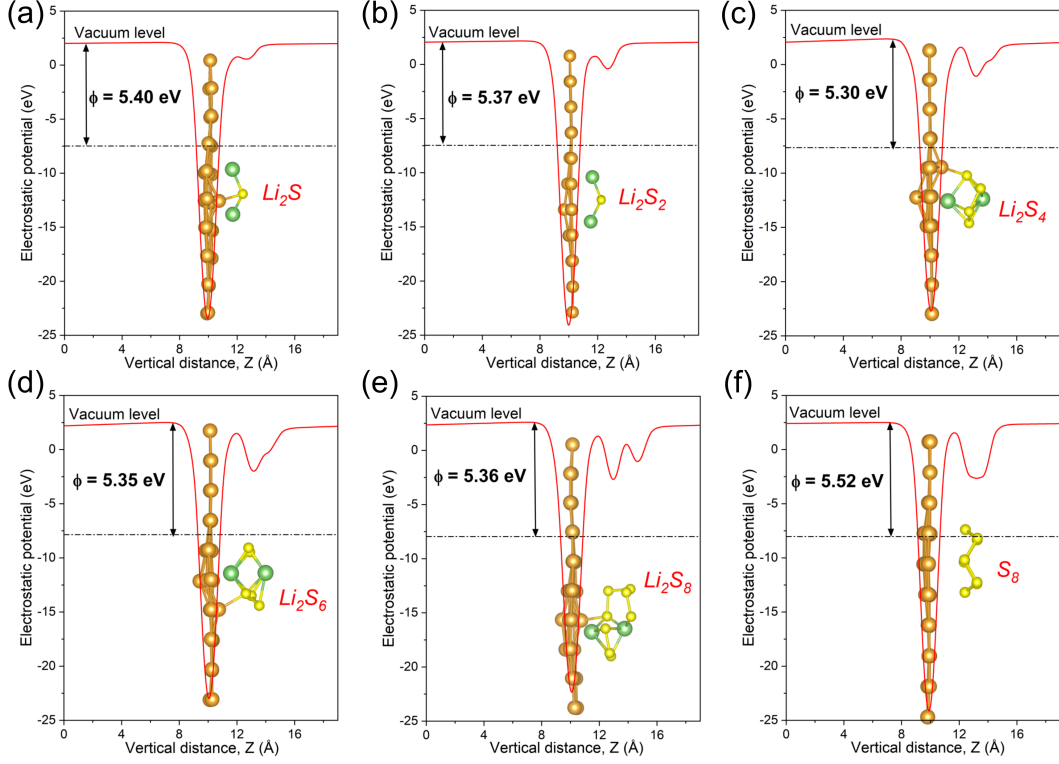


Figure 7: Planar-averaged electrostatic potential profiles along the surface normal for Goldene with adsorbed Li_2S_n and S_8 clusters. Panels (a)–(f) correspond to Li_2S , Li_2S_2 , Li_2S_4 , Li_2S_6 , Li_2S_8 , and S_8 , respectively. The work function (ϕ) for pristine Goldene is found to be 5.50 eV.

analysis is essential for improving the understanding of SRR kinetics, as a favorable free energy profile indicates thermodynamically viable Li–S bond cleavage and enhanced Li diffusion at the electrode interface.

The catalytic kinetics of the sulfur reduction reaction (SRR) on Goldene are illustrated in Fig. 8. Negative ΔG values indicate spontaneous reaction steps, whereas positive ΔG values correspond to endothermic processes that require an external potential to proceed. The conversion from S_8^* to Li_2S_8^* is highly exothermic ($\Delta G = -3.64$ eV), which is expected due to electron injection in the initial reduction step, promoting the combination of Li atoms with sulfur chains. In contrast, the intermediate conversion steps are entirely endothermic, with energy barriers of 0.23 eV ($\text{Li}_2\text{S}_8^* \rightarrow \text{Li}_2\text{S}_6^*$), 0.39 eV ($\text{Li}_2\text{S}_6^* \rightarrow \text{Li}_2\text{S}_4^*$), and 0.03 eV ($\text{Li}_2\text{S}_4^* \rightarrow \text{Li}_2\text{S}_2^*$). This trend is commonly observed and arises from the progressive cleavage of S–S bonds as the polysulfide chains shorten, a process that requires increasing energy input [47, 48]. Notably, the final conversion step to form Li_2S ($\text{Li}_2\text{S}_2^* \rightarrow \text{Li}_2\text{S}^*$) exhibits the highest free-energy barrier, at $\Delta G = 0.47$ eV, identifying this step as the rate-determining step (RDS) of the SRR on Goldene. The maximum energy barrier observed on Goldene is lower than those reported for Mo_2CS_2 (0.83 eV) [49], Janus-type Ga_2SSe (0.94 eV), and Al_2SSe (1.05 eV) [50], as well as HDG-graphene (0.68 eV) [51]. These results confirm a moderate binding strength between lithium polysulfides and the Goldene monolayer, which enables effective anchoring while avoiding excessively strong adsorption that could lead to reaction hysteresis. In general, prohibitively high energy barriers during the SRR are indicative of strong chemisorption, which hampers polysulfide conversion by impeding desorption and slowing the overall charge–discharge process.

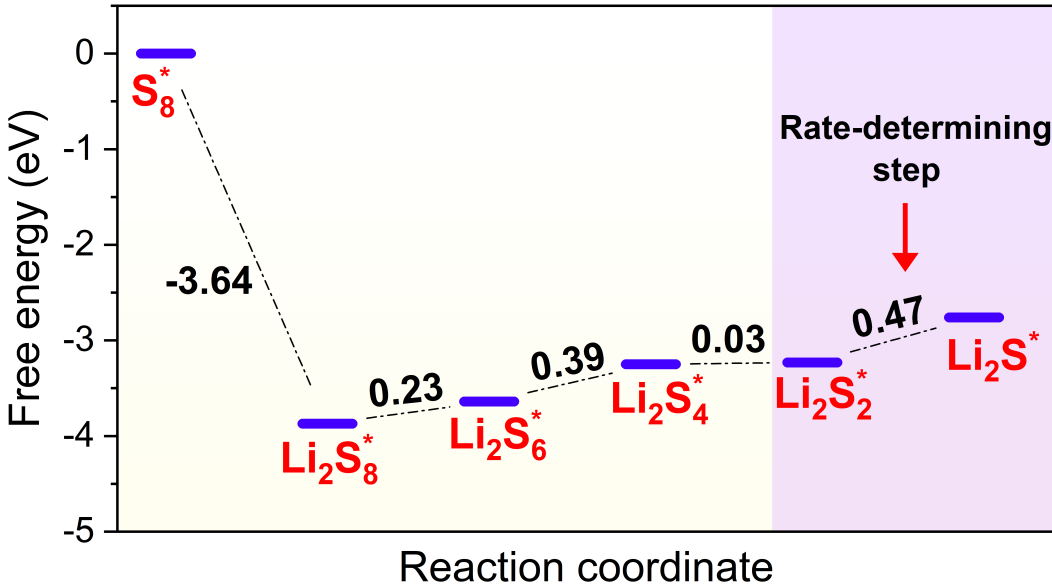


Figure 8: Reaction free energy profile for the stepwise lithiation of sulfur on the Goldene surface. The pathway illustrates the conversion from S_8 to Li_2S through successive polysulfide intermediates, Li_2S_8 , Li_2S_6 , Li_2S_4 , and Li_2S_2 . Energy values are referenced to the initial state, and the final Li_2S_2 to Li_2S transformation is identified as the rate determining step with a barrier of 0.47 eV.

4 Conclusion

In summary, we systematically investigated the interactions between lithium polysulfide species and Goldene using first-principles calculations. All Li_2S_n clusters exhibit strong adsorption on the Goldene monolayer, with adsorption energies ranging from -4.29 to -1.90 eV. These values are significantly stronger than the binding energies with common electrolyte solvents, demonstrating that Goldene is an effective substrate for anchoring lithium polysulfides. Charge-transfer analysis reveals substantial electron transfer from the Li-containing species to Goldene, reaching up to 0.92 e. This charge redistribution induces a strong interfacial dipole and reduces the work function of Goldene, indicating efficient modulation of surface reactivity upon lithium polysulfide adsorption.

Projected density of states (PDOS) calculations show that Goldene preserves its metallic character after adsorption. The Au d states remain located at the Fermi level, and the pronounced hybridization between Au d and S p orbitals suggests moderate chemical bonding at the interface. Reaction free energy analysis further indicates that sulfur lithiation on Goldene is thermodynamically favorable. The overall stabilization energy reaches -3.64 eV, and the rate-determining barrier for the Li_2S_2 to Li_2S conversion is 0.47 eV, which is lower than that reported for conventional catalysts. This favorable Gibbs free energy profile suggests enhanced reaction kinetics for the sulfur reduction reaction (SRR) on the Goldene monolayer.

Overall, these results demonstrate that Goldene is a chemically active and electronically stable two-dimensional (2D) substrate capable of strongly binding lithium polysulfides and facilitating their structural transformation. Consequently, Goldene shows considerable promise for next-generation Li-S battery applications.

Data Availability

All data supporting the findings of this study are available within the article.

Conflicts of interest

The authors declare that they have no conflict of interest.

Acknowledgments

This work was supported by the Brazilian funding agencies Fundação de Amparo à Pesquisa do Estado de São Paulo–FAPESP, grants 2024/21870-8, 2022/16509-9, and 2024/05087-1), and National Council for Scientific, Technological Development–CNPq, grant no. 307213/2021–8. L.A.R.J acknowledges financial support from FAPDF-PRONEM grant 00193.00001247 /2021-20, PDGF-FAPDF-CAPES Centro-Oeste grant number 00193-00000867/2024-94, and CNPq grants 301577/2025-0 and 444111/2024-7.

References

- [1] Yi Guo, Qian Niu, Fei Pei, Qian Wang, Yun Zhang, Liyu Du, Yin Zhang, Yunsheng Zhang, Yueying Zhang, Ling Fan, et al. Interface engineering toward stable lithium–sulfur batteries. *Energy & Environmental Science*, 17(4):1330–1367, 2024.
- [2] Yatao Liu, Yuval Elias, Jiashen Meng, Doron Aurbach, Ruqiang Zou, Dingguo Xia, and Quanquan Pang. Electrolyte solutions design for lithium-sulfur batteries. *Joule*, 5(9):2323–2364, 2021.
- [3] Youzhang Huang, Liang Lin, Chengkun Zhang, Lie Liu, Yikai Li, Zhensong Qiao, Jie Lin, Qilong Wei, Laisen Wang, Qingshui Xie, et al. Recent advances and strategies toward polysulfides shuttle inhibition for high-performance li–s batteries. *Advanced Science*, 9(12):2106004, 2022.
- [4] Jiani Wang, Hailong Wang, Songyan Jia, Qin Zhao, Qiang Zheng, Yali Ma, Tianyi Ma, and Xue Li. Recent advances in inhibiting shuttle effect of polysulfide in lithium-sulfur batteries. *Journal of Energy Storage*, 72:108372, 2023.
- [5] Xue Chen, Haijin Ji, Zhixiang Rao, Lixia Yuan, Yue Shen, Henghui Xu, Zhen Li, and Yunhui Huang. Insight into the fading mechanism of the solid-conversion sulfur cathodes and designing long cycle lithium–sulfur batteries. *Advanced Energy Materials*, 12(1):2102774, 2022.
- [6] Milan Jana, Rui Xu, Xin-Bing Cheng, Jeong Seok Yeon, Jae Min Park, Jia-Qi Huang, Qia ng Zhang, and Ho Seok Park. Rational design of two-dimensional nanomaterials for lithium–sulfur batteries. *Energy & Environmental Science*, 13(4):1049–1075, 2020.
- [7] Ke Fan and Haitao Huang. Two-dimensional host materials for lithium-sulfur batteries: A review and perspective. *Energy Storage Materials*, 50:696–717, 2022.
- [8] Imran Muhammad, Shehzad Ahmed, Zhen Yao, Danish Khan, Tanveer Hussain, and Yang-Gang Wang. First-row transition metal carbide nanosheets as high-performance cathode materials for lithium–sulfur batteries. *Nanoscale*, 16(1):262–272, 2024.
- [9] Nicolas F Martins, Warda Elaggoune, José AS Laranjeira, Yusuf Zuntu Abdullahi, and Julio R Sambrano. Anchoring performance of metallic penta-pbn monolayer in lithium-sulfur (li-s) batteries. *FlatChem*, page 100895, 2025.
- [10] Tian Yang, Jun Xia, Zhihong Piao, Lin Yang, Shichao Zhang, Yalan Xing, and Guangmin Zhou. Graphene-based materials for flexible lithium–sulfur batteries. *ACS nano*, 15(9):13901–13923, 2021.
- [11] Hiba Khaled Al-Jayyousi, Muhammad Sajjad, Kin Liao, and Nirpendra Singh. Two-dimensional biphenylene: a promising anchoring material for lithium-sulfur batteries. *Scientific Reports*, 12(1):4653, 2022.

[12] Nicolas F Martins, Yusuf Zuntu Abdullahi, José AS Laranjeira, and Julio R Sambrano. Exploring irida-graphene as an efficient anchoring material for lithium-sulfur batteries: A dft study. *Surfaces and Interfaces*, page 107193, 2025.

[13] Ting-Zheng Hou, Xiang Chen, Hong-Jie Peng, Jia-Qi Huang, Bo-Quan Li, Qiang Zhang, and Bo Li. Design principles for heteroatom-doped nanocarbon to achieve strong anchoring of polysulfides for lithium–sulfur batteries. *Small*, 12(24):3283–3291, 2016.

[14] Tapas Kuila, Saswata Bose, Ananta Kumar Mishra, Partha Khanra, Nam Hoon Kim, and Joong Hee Lee. Chemical functionalization of graphene and its applications. *Progress in Materials Science*, 57(7):1061–1105, September 2012. ISSN 0079-6425. doi:10.1016/j.pmatsci.2012.03.002. URL <http://dx.doi.org/10.1016/j.pmatsci.2012.03.002>.

[15] Da Chen, Hongbin Feng, and Jinghong Li. Graphene oxide: Preparation, functionalization, and electrochemical applications. *Chemical Reviews*, 112(11):6027–6053, August 2012. ISSN 1520-6890. doi:10.1021/cr300115g. URL <http://dx.doi.org/10.1021/cr300115g>.

[16] Alex Yong Sheng Eng, Jian Liang Cheong, and Su Seong Lee. Controlled synthesis of transition metal disulfides (mos2 and ws2) on carbon fibers: effects of phase and morphology toward lithium–sulfur battery performance. *Applied Materials Today*, 16:529–537, 2019.

[17] Ziwei Jeffrey Yang, Zhuangnan Li, Giulio I Lampronti, Jung-In Lee, Yan Wang, Jason Day, and Manish Chhowalla. Environmental and thermal stability of chemically exfoliated li x mos2 for lithium–sulfur batteries. *Chemistry of Materials*, 36(9):4829–4837, 2024.

[18] Qian Zhao, Qizhen Zhu, Yu Liu, and Bin Xu. Status and prospects of mxene-based lithium–sulfur batteries. *Advanced Functional Materials*, 31(21):2100457, 2021.

[19] Youquan Zhang, Cheng Ma, Weitao He, Chunxiao Zhang, Liangjun Zhou, Gao Wang, and Weifeng Wei. Mxene and mxene-based materials for lithium-sulfur batteries. *Progress in Natural Science: Materials International*, 31(4):501–513, 2021.

[20] Lin Liang, Liqun Niu, Tianli Wu, Dan Zhou, and Zhubing Xiao. Fluorine-free fabrication of mxene via photo-fenton approach for advanced lithium–sulfur batteries. *ACS nano*, 16(5):7971–7981, 2022.

[21] Min Fang, Jiawei Han, Shiyu He, Ji-Chang Ren, Shuang Li, and Wei Liu. Effective screening descriptor for mxenes to enhance sulfur reduction in lithium–sulfur batteries. *Journal of the American Chemical Society*, 145(23):12601–12608, 2023.

[22] Nicolas F Martins, Refilwe Edwin Mapasha, Chewe Fwalo, Warda Elaggoune, José AS Laranjeira, and Julio R Sambrano. Investigating the catalytic performance of nb2s2c tmcc monolayer for lithium-sulfur batteries. *Colloids and Surfaces A: Physicochemical and Engineering Aspects*, page 138740, 2025.

[23] Shrish Nath Upadhyay and Jayant K Singh. Unraveling the catalytic potential of 2d nb2se2c for lithium polysulfide conversion: A dft study. *ACS Applied Energy Materials*, 8(10):6733–6745, 2025.

[24] Shun Kashiwaya, Yuchen Shi, Jun Lu, Davide G Sangiovanni, Grzegorz Greczynski, Martin Magnuson, Mike Andersson, Johanna Rosen, and Lars Hultman. Synthesis of goldene comprising single-atom layer gold. *Nature Synthesis*, 3(6):744–751, 2024.

[25] Kamal Kumar, Abhishek Dhasmana, Nora de Leeuw, Jost Adam, and Abhishek K Mishra. Co2 activation on metal-and non-metal-doped goldene sheets: A dft study. *Applied Surface Science*, page 164509, 2025.

[26] Marcelo L Pereira, Emanuel JA Dos Santos, Luiz A Ribeiro, and Douglas S Galvão. How does goldene stack? *Materials Horizons*, 12(4):1144–1154, 2025.

[27] Emanuel JA dos Santos, Rodrigo AF Alves, Alexandre C Dias, Marcelo L Pereira Jr, Douglas S Galvão, and Luiz A Ribeiro Jr. Exploring novel 2d analogues of goldene: Electronic, mechanical, and optical properties of silverene and copperene. *ACS Omega*, 2025.

[28] Bohayra Mortazavi. Goldene: An anisotropic metallic monolayer with remarkable stability and rigidity and low lattice thermal conductivity. *Materials*, 17(11):2653, 2024.

[29] Rong Zou, Jie Zhang, Yawen Zheng, Jinling Li, Wenwu Liu, and Fen Ran. Tailoring interfacial electric field by gold nanoparticles enable electrocatalytic lithium polysulfides conversion for lithium-sulfur batteries. *Small*, 20(29):2312102, 2024.

[30] Kai Sun, Yujun Fu, Taishu Sekine, Haruna Mabuchi, Sakiat Hossain, Qiang Zhang, Dequan Liu, Saikat Das, Deyan He, and Yuichi Negishi. Metal nanoclusters as a superior polysulfides immobilizer toward highly stable lithium–sulfur batteries. *Small*, 20(2):2304210, 2024.

[31] Chun-Ying Chao, Long-Yang Zhang, Jing-Qi Wang, Pin-Jiang Li, Hong-Wei Yue, Li-Jun Wu, and Hao Li. Leveraging spontaneous polarization and catalysis: Pbtio3@ au composites for suppressing the lips shuttle effect in lithium-sulfur batteries. *Ionics*, pages 1–11, 2025.

[32] G. Kresse and D. Joubert. From ultrasoft pseudopotentials to the projector augmented-wave method. *Physical Review B*, 59(3):1758–1775, January 1999. ISSN 1095-3795. doi:10.1103/physrevb.59.1758. URL <http://dx.doi.org/10.1103/PhysRevB.59.1758>.

[33] P. E. Blöchl. Projector augmented-wave method. *Physical Review B*, 50(24):17953–17979, December 1994. ISSN 1095-3795. doi:10.1103/physrevb.50.17953. URL <http://dx.doi.org/10.1103/PhysRevB.50.17953>.

[34] John P Perdew. Generalized gradient approximations for exchange and correlation: A look backward and forward. *Physica B: Condensed Matter*, 172(1-2):1–6, 1991. doi:10.1016/0921-4526(91)90409-8. URL [http://dx.doi.org/10.1016/0921-4526\(91\)90409-8](http://dx.doi.org/10.1016/0921-4526(91)90409-8).

[35] John P. Perdew, Kieron Burke, and Matthias Ernzerhof. Generalized gradient approximation made simple. *Physical Review Letters*, 77(18):3865–3868, October 1996. ISSN 1079-7114. doi:10.1103/physrevlett.77.3865. URL <http://dx.doi.org/10.1103/PhysRevLett.77.3865>.

[36] Stefan Grimme, Jens Antony, Stephan Ehrlich, and Helge Krieg. A consistent and accurate ab initio parametrization of density functional dispersion correction (dft-d) for the 94 elements h-pu. *The Journal of chemical physics*, 132(15), 2010.

[37] Chou Wu, Shaobo Jia, Haiyan Zhu, Jianxiao Shang, Tingting Li, Shanlin Chen, Zhequn Ren, Ghulam Meeladi, Bingbing Suo, Wenli Zou, et al. ds/p orbital hybridization-driven synergy in heteronuclear dual-atom catalysts on cn/c2n for high-efficiency lithium-sulfur batteries. *Carbon*, page 120862, 2025.

[38] Bin Yu, Qiu He, and Yan Zhao. Exploring the anchoring effect and catalytic mechanism of 3d transition metal phthalocyanine for s8/lipss: A density functional theory study. *Applied Surface Science*, 558:149928, 2021.

[39] Qing-Wen Zeng, Ri-Ming Hu, Zhi-Bin Chen, and Jia-Xiang Shang. Single-atom fe and n co-doped graphene for lithium-sulfur batteries: a density functional theory study. *Materials Research Express*, 6(9):095620, 2019.

[40] Patricio Vélez, María del Carmen Rojas, Juan Velasco, María Laura Para, Daniel Barraco, Ezequiel PM Leiva, and Guillermina L Luque. On the role of oxidized graphene interfaces in lithium sulfur batteries: Thermodynamic and kinetic aspects using density functional theory. *Applied Surface Science*, 550:149358, 2021.

[41] Xue-li Li and Dong-Xing Song. Anchoring enhancement of graphdiyne by doping and molecular intercalation for lithium- sulfur batteries. *Journal of Electroanalytical Chemistry*, 988:119131, 2025.

[42] Jiahui Yu, Yichen Jin, Minglang Hu, Wei Ren, Yiqun Xie, and Yin Wang. Bc6n as a promising sulfur host material for lithium-sulfur batteries. *Applied Surface Science*, 577:151843, 2022.

[43] Meng Zhao, Hong-Jie Peng, Bo-Quan Li, and Jia-Qi Huang. Kinetic promoters for sulfur cathodes in lithium–sulfur batteries. *Accounts of Chemical Research*, 57(4):545–557, 2024.

[44] Zhihua Wang, Junru Ke, He Zhu, Fan Xue, Jun Jiang, Wen Huang, Min Dong, Xindong Zhu, Jianrong Zeng, Ruoyu Song, et al. Steric hindrance-induced amorphous lithium sulfide deposition accelerates sulfur redox kinetics in lithium–sulfur batteries. *Advanced Materials*, page 2504715, 2025.

- [45] Nicolas F Martins, José A Laranjeira, Pablo A Denis, and Julio R Sambrano. High sensitivity of nitrobenzene on the zno monolayer and the role of strain engineering. *Applied Surface Science*, 679:161280, 2025.
- [46] Warda Elaggoune, Nicolas F Martins, Julio R. Sambrano, and Yusuf Zuntu Abdullahi. Enhancing so₂ and no₂ gas sensing using zncdo₂-based porous nanosheets: A dft perspective. *ACS omega*, 10(33):37974–37984, 2025.
- [47] Feiran Liu, Ning Wang, Chunsheng Shi, Junwei Sha, Liying Ma, Enzuo Liu, and Naiqin Zhao. Phosphorus doping of 3d structural mos₂ to promote catalytic activity for lithium-sulfur batteries. *Chemical Engineering Journal*, 431:133923, 2022.
- [48] Gaoran Li, Shun Wang, Yining Zhang, Matthew Li, Zhongwei Chen, and Jun Lu. Revisiting the role of polysulfides in lithium–sulfur batteries. *Advanced Materials*, 30(22):1705590, 2018.
- [49] Na Li, Jun Fan, and Jianfeng Jia. Adsorption-catalysis mechanism of non-noble single transition metal atom immobilized on mo₂cs₂ mxene as sulfur hosts for lithium- sulfur batteries. *Journal of Power Sources*, 640:236783, 2025.
- [50] Zhiwei Li, Qingyi Feng, Taiyu Hao, Bo Li, Xia Xiang, Sean Li, Hongxiang Deng, Wei Liu, and Xiaotao Zu. Janus-type monolayer m2sse (m= ga, in, b, and al) as sulfur host materials for lithium-sulfur batteries: A first-principles study. *Journal of Power Sources*, 625:235629, 2025.
- [51] Han Wang, Zonggang Qiu, Jiyuan Guo, Huabing Shu, and Qin Wei. Unravelling the anchoring effects of hd-graphene for lithium-sulfur batteries: A first-principles calculation. *Journal of Energy Storage*, 90:111842, 2024.